ORGANOMETALLICS
ARTICLE
pubs.acs.org/Organometallics

Engineering Femtosecond Organometallic Chemistry: Photochemistry and Dynamics of Ultrafast Chelation of Cyclopentadienylmanganese Tricarbonyl Derivatives with Pendant Benzenecarbonyl and Pyridinecarbonyl Groups

Edwin J. Heilweil,[‡] Jermaine O. Johnson,[†] Karen L. Mosley,[†] Philippe P. Lubet,[†] Charles Edwin Webster,[*,†] and Theodore J. Burkey[*,†]

[†]Department of Chemistry, The University of Memphis, Memphis, Tennessee 38152-3550, United States

[‡]Optical Technology Division, Physics Laboratory, National Institute of Standards and Technology, Gaithersburg, Maryland 20899-8443, United States

Ⓢ *Supporting Information*

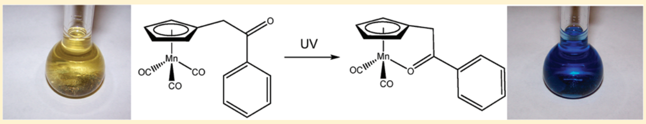

ABSTRACT: The chelation following photodissociation of CO for cyclopentadienyl manganese tricarbonyl derivatives with a bifunctional side chain has been investigated. Previous studies show that steady-state irradiation of **1** (Mn{η^5-$C_5H_4CH_2COR$}-$(CO)_3$, R = 2-pyridyl) leads to CO dissociation and formation of *O*-chelate **2** with smaller amounts of *N*-chelate **3**. Subsequently, **2** rearranges thermally to **3**. A new preparation for **1** is reported, while analogues **4** (R = phenyl) and **5** (R = 4-pyridyl) are prepared for the first time. Steady-state UV−vis, FTIR, and NMR studies of **4** and **5** in heptane demonstrate that *O*-chelates **6** and **7**, respectively, are formed with the side-chain oxygen but decay on the minute time scale. The linkage isomerization of *O*-chelate **2** to **3** is faster than the decay observed for the *O*-chelate **6** (R = 2-pyridyl versus Ph), even in the presence of 0.1 M pyridine for the latter. Following irradiation of **4** during time-resolved infrared studies in heptane, ultrafast *O*-chelation is observed but not ultrafast solvent coordination. Ultrafast *O*-chelation is also observed for **5** along with an unidentified transient. Following irradiation of **1**, ultrafast *O*- and *N*-chelation are observed, to the exclusion of ultrafast solvent coordination. This result suggests that chelate formation is a subpicosecond process and that both chelates are formed independently. A split in the otherwise degenerate stretching bands for **4** and **5** in FTIR spectra suggests that there is significant electronic communication between the side chain and the metal carbonyl groups. The results suggest that ultrafast chelation is favored by side-chain conformations that position a functional group near the metal center.

■ INTRODUCTION

When a coordinated functional group is part of a chelate ring, strain and conformational restrictions can be expected to affect bond energies, vibrational and electronic transitions, and the rates of addition or dissociation of the functional group. We are interested in designing efficient photochromic organometallics based on the mechanism of a photoreversible linkage isomerization where chelation following the photodissociation of a ligand is a key process. Understanding how structural features influence chelate stability or its rate of formation is invaluable for this project.[1] An early study of photochelation reported that a series of $CpMn(CO)(\eta^1\text{-P−P})$, where P−P were diphosphines, all formed four- to six-membered rings within 100 ns following irradiation.[2] The quantum yield (0.6) for chelate formation was independent of ring size, indicating that the product-determining step preceded chelation. In contrast, the quantum yield for chelation of $(\eta^5\text{-}C_5H_4R)Mn(CO)_3$ (R = $COCH_2OCH_3$, $COCH_2SCH_3$, $CO(CH_2)_2SCH_3$, $CH_2CO_2CH_3$, $(CH_2)_2CO_2CH_3$) varied with the structure of R (0.6−1.0),[3] and the rates of chelation varied from 2×10^6 to greater than 5×10^9 s^{-1}.[4,5]

In many cases photochelation competes with ultrafast ligand recombination and solvent coordination, which occur in a picosecond or less.[6] Our studies have shown that chelation generally occurs on two time scales.[4,5] The first time scale is subpicosecond, where chelation competes with ligand recombination and solvent coordination. For some compounds the chelation occurs to the exclusion of both ligand recombination and solvent coordination even when a solvent such as acetonitrile makes strong and kinetically stable bonds with the metal center.[5a] The second time scale is about 100 ns for species in alkane solvents where a coordinated solvent molecule must be displaced for chelation to occur. The time scale is often longer in more reactive solvents where a strongly coordinated solvent must be displaced. Since ultrafast solvent coordination and ligand recombination can lead to unproductive processes and delays for light-driven molecular devices, it is important to understand how these processes can be eliminated.

UV irradiation of cyclopentadienyl manganese tricarbonyl derivatives with pendant functional groups leads to chelate formation

Received: May 2, 2011
Published: October 24, 2011

dx.doi.org/10.1021/om2003656 | *Organometallics* 2011, 30, 5611–5619

Scheme 1. The Photochrome 2/3 Produced Following Irradiation of 1

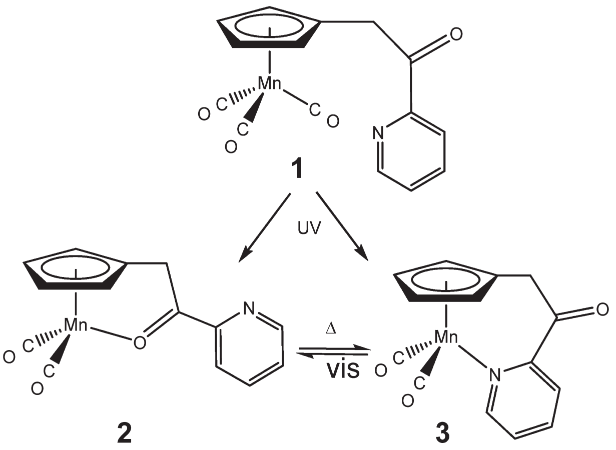

Scheme 2

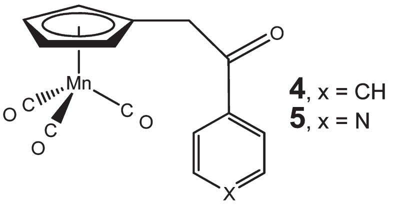

for esters,[3] sulfides,[3] pyridines,[7] ketones,[7] nitriles,[8] alkenes,[8] alkynes,[8] and carbamates.[9] In the case of **1** (Scheme 1), a photochrome[10] is produced based on blue (**2**) and purple (**3**) linkage isomers.[7] **2** is unstable at room temperature and rearranges to **3** within 5 min but can be reversed by irradiation with visible light. At the lowest temperatures and shortest irradiation times, the ratio of **2** to **3** increases to 3:1 and suggests that irradiation initially favors the formation of **2**. An important issue is the extent that both isomers are formed from an excited state directly, or by photoisomerization via secondary photolysis, or by thermal isomerization following irradiation. In this study, steady-state irradiation studies of analogues that are not capable of forming an *N*-chelate (**4** and **5**, Scheme 2) and ultrafast, time-resolved infrared studies (TRIR) of **1**, **4**, and **5** are used to identify transient species following irradiation, to understand the selectivity for isomer formation, and to measure isomerization rates.

■ EXPERIMENTAL SECTION

General Conditions. Unless otherwise noted, all reactions were carried out under nitrogen or argon in a glovebox or Schlenk flask, and all steady-state irradiations were conducted with a single RPR-3000 UV lamp (Southern New England Ultraviolet Company) or Pen Ray lamp (UVP). Infrared spectra were obtained with a Thermo Nicolet 380. UV—vis spectra were obtained with an Agilent 8453 spectrophotometer (A_0 = absorbance at time = 0, A_t = absorbance at time t).[11]

Synthesis of 1, Tricarbonyl[η^5-(2-oxo-2-pyridyl)ethyl)cyclopentadienyl]manganese. Potassium *tert*-butoxide (6.1 g, 55 mmol) was dissolved in anhydrous DMF (20 mL) in a 100 mL Schlenk flask, followed by methyl cymantrene (5 mL, 32 mmol) and argon-purged ethyl picolinate (5 mL, 35 mmol). After stirring for 12 h, 50 mL of nitrogen-purged 1.2 M HCl was cannulated into the flask. Sodium bicarbonate (5%, 10 mL) was added, and the solution was extracted with three 50 mL aliquots of diethyl ether. The combined ether layers were back-extracted with two 50 mL aliquots of water and dried overnight with magnesium sulfate. The ether was reduced by 30% before recrystallization at 4 °C (4.92 g, 52% yield). ^{1}H NMR (270 MHz, $CDCl_3$): δ (ppm) 4.20 (s, 2 H, CH_2), 4.67 (m, 2 H, 3,4-Cp), 4.85 (m, 2 H, 2,5-Cp), 7.49 (m, 1 H, 5-py), 7.84 (m, 1 H, 4-py), 8.05 (m, 1 H, 3-py), 8.70 (m, 1 H, 6-py).

Synthesis of 4, Tricarbonyl[η^5-(2-oxo-2-phenyl)ethyl)cyclopentadienyl]manganese. The procedure was the same as for **1** except where noted: potassium *tert*-butoxide (4.5 g, 40 mmol), methyl cymantrene (6.3 mL, 40 mmol), and ethyl benzoate (7.1 mL, 50 mmol) instead of ethyl picolinate. The mixture was stirred for 24 h. The ether was evaporated with a nitrogen stream to provide a solid product, which was dissolved in 150 mL of anhydrous diethyl ether outside the glovebox. The solution was washed with water (3 × 25 mL), dried with $MgSO_4$, filtered, and gradually cooled to −16 °C. A yellow product formed overnight (1.56 g, 32%). Overall yield: 23%. Elemental analysis found for $C_{16}H_{11}MnO_4$, MW = 322.19: analysis (calculated) C 59.45 (59.64) H 3.80 (3.44). ^{1}H NMR (270 MHz, $CDCl_3$): δ (ppm) 3.94 (s, 1 H), 4.72 (m, 2 H), 4.78 (m, 2 H), 7.49 (t, J = 7.4 Hz, 2 H), 7.60 (t, J = 7.4 Hz, 1 H), and 7.98 (d, J = 7.4 Hz, 2 H). ^{13}C NMR (67.5 MHz, $CDCl_3$): δ (ppm) 37.79, 82.25, 84.43, 97.35, 128.43, 128.97, 133.78, 136.09, 195.92, and 225.07. FTIR (NaCl, heptane): 2024 (4 cm^{-1} fwhm), 1946 and 1938 cm^{-1} (apparent 13 cm^{-1} fwhm for overlapping peaks).

Synthesis of 5. Tricarbonyl[η^5-(2-oxo-2-(4-pyridyl)ethyl)-cyclopentadienyl]manganese. The procedure was the same as for **1** except where noted: potassium *t*-butoxide (2.3 g, 20.5 mmol), methyl cymantrene (2.5 mL, 14.7 mmol), and ethyl isonicotinate (1.8 mL, 13.4 mmol) instead of ethyl picolinate. After workup, the solid residue was crystallized in 30 mL of argon-purged toluene (2.12 g, 49% yield). Elemental analysis found for $C_{15}H_{10}MnNO_4$, MW = 323.18 (calculated): C 55.78 (55.75) H 3.02 (3.12) N 4.29 (4.33). ^{1}H NMR (270 MHz, $CDCl_3$): δ (ppm) 3.97 (s, 2 H, CH_2), 4.76 (br s, 2 H, 3,4-Cp), 4.81 (br s, 2 H, 2,5-Cp), 7.77 (d, 5.0 Hz, 2 H, 3,5 pyr), 8.87 (d, 5.0 Hz, 2 H, 2,6 pyr). ^{13}C NMR (67.5 MHz, $CDCl_3$): δ (ppm) 38.02, 82.45, 84.49, 95.79, 121.23, 141.95, 151.37, 195.48, and 225.00. FTIR (NaCl, heptane): 2026 (4 cm^{-1} fwhm), 1949 and 1940 cm^{-1} (apparent 17 cm^{-1} fwhm for overlapping peaks).

Ligand Substitution of *O*-Chelate from 4 with Pyridine Monitored via UV—Vis Spectroscopy. In a typical experiment, a solution of **4** (3.2 mg) in 10 mL of heptane (1 mM) was stirred overnight in a glovebox. Two milliliters were transferred to a quartz screw cap cuvette (l = 1 cm), and a UV—vis spectrum was recorded. The cuvette was positioned 5 cm from an RPR-3000 lamp and irradiated (60 s) until A_{635} (absorbance at 365 nm) reached 1.0 OD. The pyridine concentration was brought to 10 mM by injecting 10 μL of 2 M pyridine into the irradiated solution, and spectra were obtained at 30 s intervals. The intercepts for Figures 7, 8, 10, and 11 are within experimental error of zero.

FTIR Spectra of Irradiated Samples. In a typical experiment, **4** (29 mg) in 10 mL of heptane (9 mM) was irradiated in a 0.1 mm path length CaF_2 cell at room temperature. The cell was irradiated for 30 s twice and then 60 s with a Pen Ray lamp. Readings were taken immediately (<5 s) after irradiation and 4 min after irradiation. The cell was positioned 10 cm away from the lamp.

TRIR Spectroscopy. The transient absorption apparatus at NIST has been described in detail previously.[5] Spectra were averaged for 1000—3000 laser shots. For **1**, nanosecond spectra were obtained following 266 nm irradiation, and picosecond spectra were obtained following 289 nm irradiation. For **4** and **5**, all picosecond and nanosecond spectra were obtained following 355 nm irradiation. In typical experiments, **1** (23 mg) was dissolved in 80 mL of heptane (0.85 mM), **4**

Scheme 3. Irradiation of 4

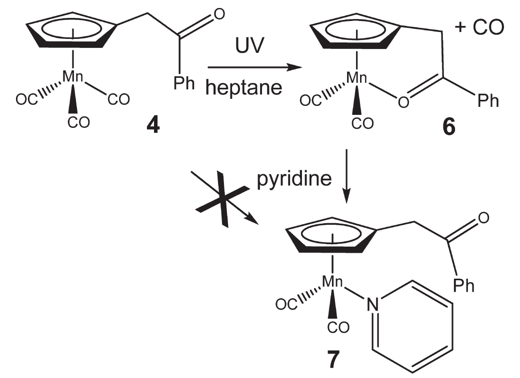

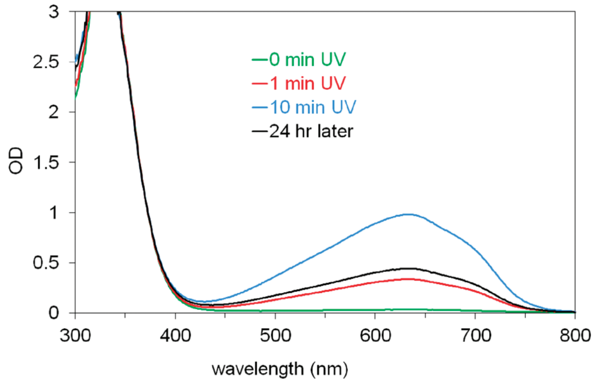

Figure 1. UV−vis spectra of 3 mM **4** in heptane at room temperature following UV irradiation.

(39 mg) in 75 mL of heptane (1.6 mM), and **5** (21 mg) in 50 mL of heptane (1.3 mM).

Computational Methods. Theoretical calculations have been carried out using the Gaussian09[12] implementation of PBEPBE (Perdew−Burke−Ernzerhof exchange correlation functional[13]) density functional theory[14] using the default pruned fine grids for energies (75, 302), default pruned coarse grids for gradients and Hessians (35, 110) (neither grid is pruned for manganese), and nondefault SCF convergence for geometry optimizations (10^{-6}). The basis set for manganese was the Hay and Wadt basis set and effective core potential combination (LANL2DZ)[15] as modified by Couty and Hall, where the two outermost p functions have been replaced by a split of the optimized 4p functions,[16] supplemented with a single set of f polarization functions.[17] The 6-31G(d′)[18,19] basis sets were used for all other atoms. The density fitting approximation[20] for the fitting of the Coulomb potential was used for all calculations; auxiliary density-fitting basis functions were generated automatically (by the procedure implemented in Gaussian 09.A02) for the specified AO basis set. Spherical harmonic d and f functions were used throughout; that is, there are five angular basis functions per d function and seven angular basis functions per f function. All structures were fully optimized, and analytical frequency calculations were performed on all structures to ensure stationary points are a zeroth-order saddle point (a local minimum), or first-order saddle point (a transition state) was achieved.

RESULTS

Synthesis. A new synthesis of **1** in DMF based on the acylation of the methyl cymantrene carbanion is a considerable improvement in yield (50%) and purification over the previous method.[7] The structure of **1** was confirmed by comparing spectra with published results. Lower yields (<30%) were obtained in DMSO, and a similar procedure using BuLi in THF at −78 °C produced no detectable product. **4** and **5** were likewise prepared in DMF, although a lower isolated yield was obtained for **4**.

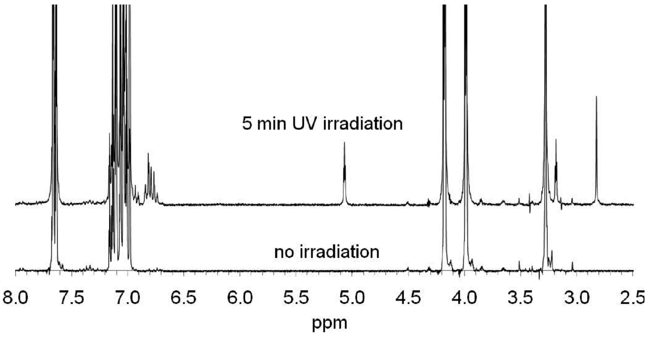

Figure 2. NMR spectra for low-temperature irradiation of **4** in toluene-d_8: (lower) at room temperature before irradiation; (upper) 5 min total irradiation at −20 °C. The probe temperature was 25 °C during acquisition.

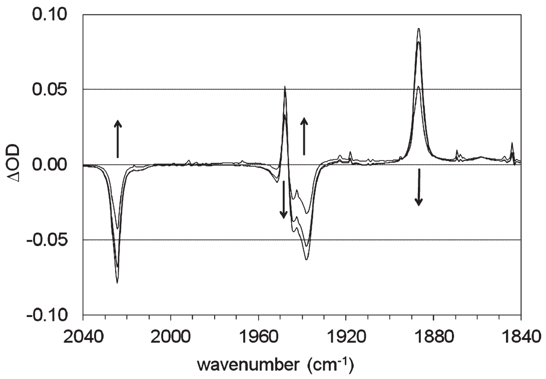

Figure 3. FTIR spectral changes after 30 s irradiation of 9 mM **4** in heptane at room temperature. Difference spectra were recorded 0, 3, and 60 min after irradiation.

Steady-State and Flash Photolysis of 4. The formation of intermediates and products following irradiation of **4** (Scheme 3 and TOC figure) were identified using UV−vis, NMR, and IR spectroscopies. A 3 mM heptane solution of **4** is faint yellow with little visible absorbance (Figure 1). UV irradiation changes the solution to blue with a peak forming at 635 nm and decaying with a half-life of 24 h at 23 °C. UV irradiation of **4** in toluene-d_8 likewise changes the solution to blue as new NMR peaks appear; some peaks are obscured by those for solvent and **4**, while peaks at 6.8, 5.1, 3.2, and 2.8 ppm are well resolved (Figure 2, area ratios of the latter three peaks are 1:1:1). UV irradiation of **4** in heptane led to bleaching of starting material peaks at 2024 and 1946/1938 cm^{-1} (overlapping) in difference FTIR spectra and new absorption peaks at 1948 and 1887 cm^{-1} (Figure 3). After 60 min in the dark at room temperature, the peaks at 1948 and 1887 cm^{-1} decreased by 50%, and the bleached peaks similarly recovered. Difference TRIR spectra for **4** reveal the peak at 1887 cm^{-1} appears in less than 100 ps with no change to 1 μs (Figure 4). In the presence of 1 mM pyridine, the bleach recovery is almost completely inhibited, but the absorption peak at 1887 cm^{-1} decays by 50% in 70 min, while two additional peaks

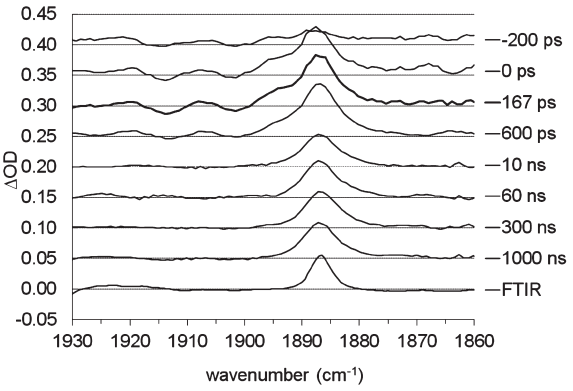

Figure 4. TRIR difference spectra acquired after 355 nm pulsed laser irradiation of 1.6 mM **4** in heptane at 25 °C. The spectra are offset vertically by 0.05 OD units. Bleaches and absorptions at higher wavenumbers were not recorded. The FTIR difference spectrum was obtained after steady-state UV irradiation.

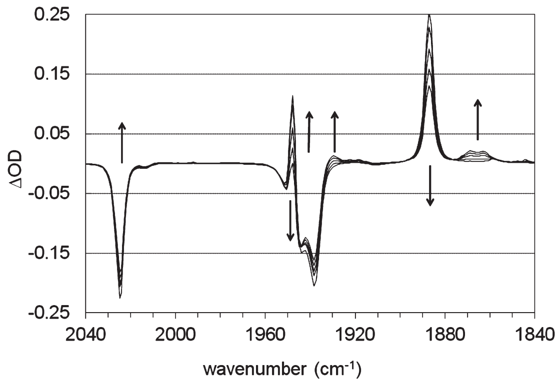

Figure 5. FTIR spectral changes after 1 min irradiation of 1 mM **4** with 1 mM pyridine in heptane at 25 °C. Difference spectra were recorded 0, 10, 30, 50, and 70 min after irradiation.

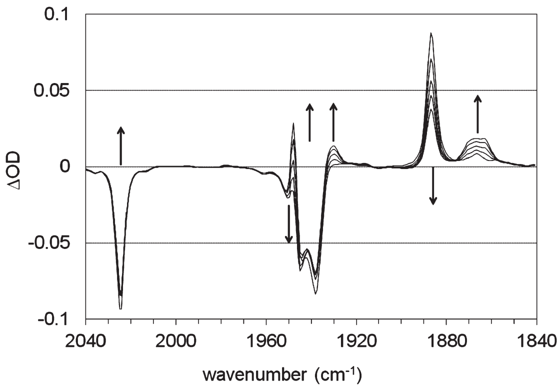

Figure 6. FTIR spectral changes after 1 min irradiation of 1 mM **4** with 10 mM pyridine in heptane at 25 °C (CaF_2, 0.95 mm). Difference spectra were recorded 0, 5, 10, 15, and 20 min after irradiation.

appear at 1932 and 1865 cm^{-1} (Figure 5). These latter peaks grow more rapidly in the presence of 10 mM pyridine, and the 50% decay of the 1887 cm^{-1} peak is also faster (20 min, Figure 6).

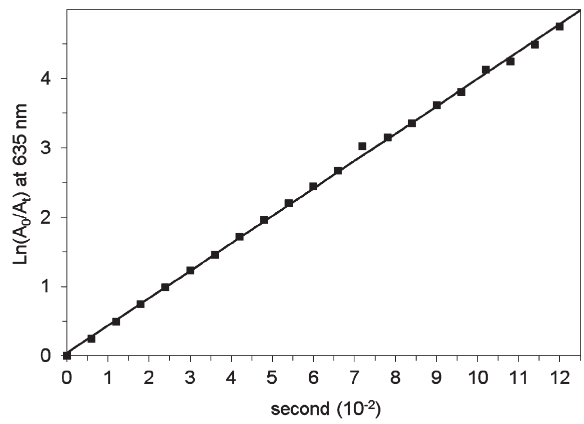

Figure 7. Plot of $\ln(A_0/A_t)$ at 635 nm after irradiation of 1 mM **4** and addition of 0.1 M pyridine in heptane. k_{obs} = 3.95(0.03) × 10^{-3} s^{-1}, R = 0.9995, baseline correction = 0.005.

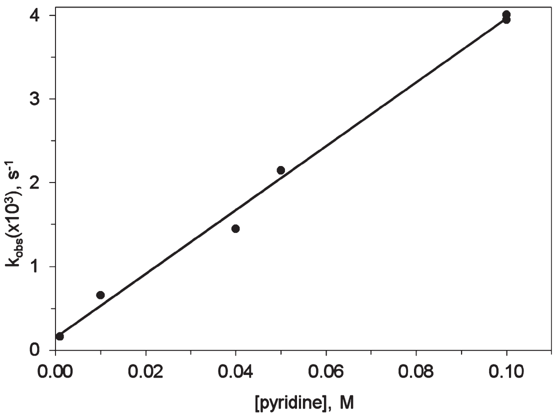

Figure 8. Plot of k_{obs} versus [pyridine] monitored at 635 nm for irradiation of **4** in heptane, k_1 = 3.8(0.2) × 10^{-2} M^{-1} s^{-1}, R = 0.997.

Rate constants for the decay of the absorption at 635 nm observed after irradiation of **4** were obtained at different concentrations of pyridine. In the absence of pyridine, the decay did not follow first- or second-order kinetics, and the rate of decay actually increased with time (Figures 1S and 2S, Supporting Information).[21] In the presence of 0.1 M pyridine, the decay of A_{635} displayed first-order kinetics (Figure 7), and an isosbestic point is observed at 476 nm (Figures 3S and 4S, Supporting Information). Plots of $\ln(A_0/A_t)$ versus time at 635 or 680 nm were linear for pyridine concentrations of 1−100 mM (Figures 5S−17S, Supporting Information). The observed rate constants obtained from the slopes of these plots were plotted versus pyridine concentration (Figure 8) to yield a slope of k_1 = 3.8(0.2) × 10^{-2} M^{-1} s^{-1}.

Steady-State and Flash Photolysis of 5. Results for **5** were similar to **4** (Scheme 4). The steady-state UV irradiation of a pale yellow solution containing **5** changed to blue as a peak at 704 nm increased with irradiation time (Figure 18S, Supporting Information) and then decreased by >50% in the dark in 30 min (Figure 9). A plot of $\ln(A_0/A_t)$ versus time for the decay at 700 nm after irradiation of **5** yielded k_{obs} = 5.1(0.1) × 10^{-4} s^{-1} in the absence of pyridine (Figure 10) and 4.9(0.1) × 10^{-4} s^{-1} in the presence of 1 mM pyridine (Figure 11). Difference FTIR spectra of **5** after UV irradiation at −10 °C reveal bleaches at 2027, 1948/1940 cm^{-1} (overlapping) and new peaks at 1952 and 1894 cm^{-1} (Figure 12). As the new peaks decay (50% in 100 min), the bleached peaks only partially recover and two new broad absorption features grow from 1907 to 1930 cm^{-1} and 1870 to 1840 cm^{-1}

Scheme 4. Irradiation of **5**

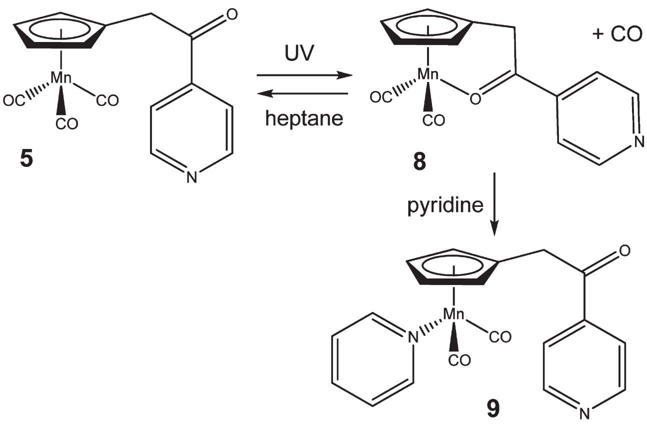

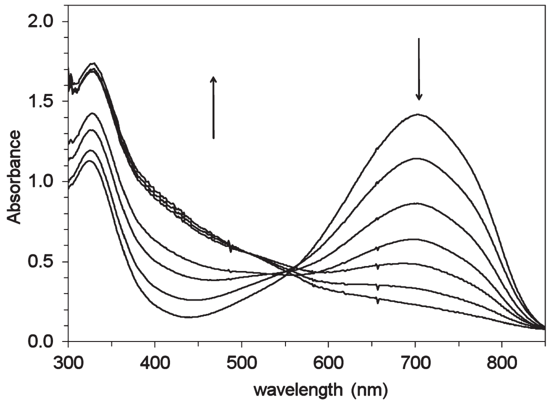

Figure 9. UV−vis spectra following irradiation of 1 mM **5** with no added pyridine in heptane at 25 °C, delay = 0, 10, 20, 30, 40, 50, and 60 min.

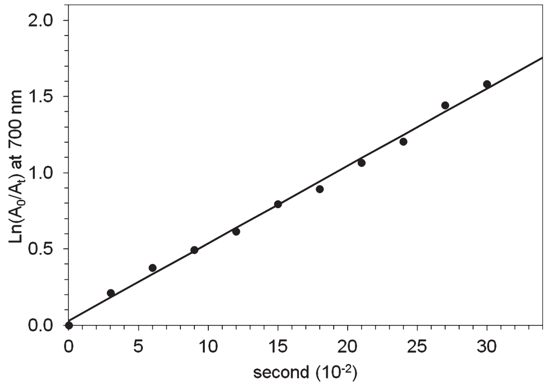

Figure 10. Plot of $\ln(A_0/A_t)$ at 700 nm following irradiation of 1 mM **5** without pyridine in heptane at 25 °C, k_{obs} = 5.1(0.1) × 10^{-4} s^{-1}, R = 0.998, first point correction.

with an apparent 20 min half-life. Similarly, TRIR spectra also reveal absorption peaks at 1952 and 1894 cm^{-1} and bleaches at 1948 and 1940 cm^{-1} (Figure 13). The peak at 1894 cm^{-1} appears completely formed within 67 ps and does not change in amplitude or shape for delays to 2 μs. The peak is asymmetric with a "shoulder" on the low-frequency side and has an apparent 12 cm^{-1} fwhm.

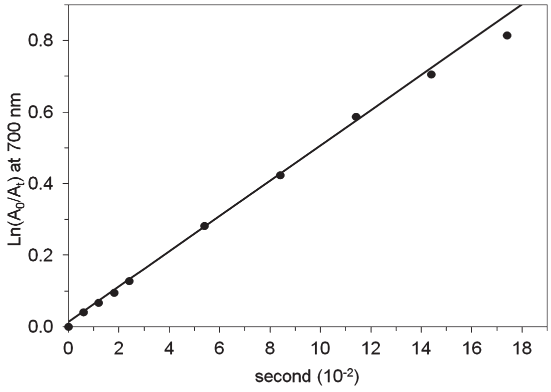

Figure 11. Plot of $\ln(A_0/A_t)$ at 700 nm following irradiation of 1 mM **5** with 1 mM pyridine in heptane at 25 °C, k_{obs} = 4.9(0.1) × 10^{-4} s^{-1}, R = 0.999, first point and baseline correction.

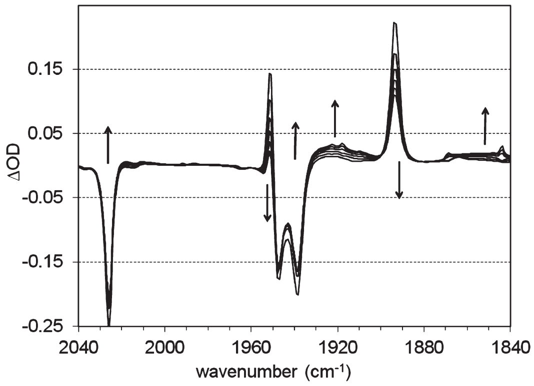

Figure 12. FTIR spectral changes following irradiation of 1 mM **5** in heptane at −10 °C. Spectra are recorded at time 0, 10, 20, 40, 60, 80, and 100 min.

Flash Photolysis of 1. Steady-state photolysis studies of **1** were reported previously.[7] TRIR spectra for **1** in heptane reveal a bleach feature near 1940 cm^{-1} and new absorption peaks at 1947, 1887, and 1878 cm^{-1} (Figure 14). The peaks are fully developed within 133 ps, where the intensity ratio of 1887 to 1878 cm^{-1} is about 3:1. This ratio does not change up to 500 ns and is the same as that initially observed at low temperature and short irradiation times in FTIR spectra.[7]

Computations of Metal-Bound CO Infrared Stretching Frequencies. Several low-energy conformations of **1**, **4**, and **5** were determined computationally, and the metal-bound CO frequencies are reported in Table 1 along with experimental results for **1**−**8** (see spectra in Supporting Information, Figures 19S−24S). As expected, the computed harmonic frequencies are blue-shifted compared to experimental frequencies, but the relative frequencies are consistent. The computed asymmetric stretching vibrations are not degenerate, and compared to **1** the difference is much larger for **4** and **5**. Stationary points and computed frequencies are also reported for **8**, related chelate isomers, and σ-ethane complexes in the Supporting Information, Scheme S1 and Tables S3 and S4. All the chelate isomers have higher computed frequencies than the computed frequencies for **8**. Only the σ-ethane complexes and coordinatively unsaturated isomers (no chelated side chains) have lower frequencies that **8**.

■ DISCUSSION

Formation and Decay of the *O*-Chelate from 4. The spectroscopic results suggest that an *O*-chelate is formed following irradiation of **4**. The electronic transition at 635 nm for a blue product along with NMR and IR peaks similar to those reported for **2** (Figures 1−6, Scheme 3, Table 1)[7] are assigned to *O*-chelate **6**. Because **4** has virtually no visible absorption (Figure 1, 0 min), the peak at 635 nm can be attributed entirely to product. The shape and peak position in the visible spectrum, including a shoulder at 700 nm, are almost identical to those reported for **2**.[22] The areas and shifts of the new NMR peaks at 5.1, 3.2, and 2.8 ppm after irradiation in toluene-d_8 (Figure 2) are assigned to the α-Cp, β-Cp, and methylene peaks of **6**, respectively, and are consistent with those observed for **2** (5.4, 4.1, and 3.3 ppm in methylcyclohexane-d_{14}) considering solvent differences and potential steric and shielding effects resulting from the presence of the phenyl group and restricted conformations of the pyridine ring. The Mn-bound CO IR frequencies of **6** (1948 and 1887 cm^{-1}, Figure 3) are nearly identical to those for **2** (1947 and 1887 cm^{-1} versus 1941 and 1878 cm^{-1} for **3**).[7] These assignments are consistent with the computational results in Table 1. In summation, the results suggest that **6** and **2** are *O*-chelates because **6** cannot be an *N*-chelate and the spectral properties for **6** are similar to **2** but distinctly different from those for **3**, where *N*-chelation is confirmed by its X-ray crystal structure.[7]

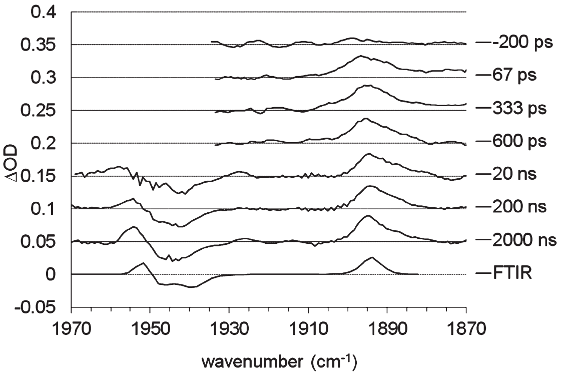

Figure 13. TRIR difference spectra acquired after 355 nm pulsed laser irradiation of 1.3 mM **5** in heptane. The spectra are offset vertically by 0.05 OD units. The FTIR difference spectrum was obtained after steady-state UV irradiation of 0.5 mM **5** in heptane.

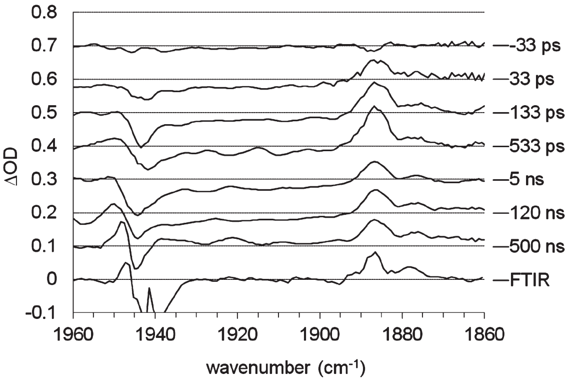

Figure 14. TRIR difference spectra acquired after pulse laser irradiation of **1** (picosecond, 266 nm, 0.9 mM; nanosecond, 289 nm, 1.4 mM). The FTIR spectrum was obtained after steady-state UV irradiation of 0.6 mM **1** in heptane.

In the absence of pyridine, the *O*-chelate **6** decays as the bleach of **4** recovers, indicating recombination with carbon monoxide. The recovery of **4** from *O*-chelate **6** can be inhibited by pyridine: minor recovery of **4** is observed as two new peaks (1932 and 1865 cm^{-1}) assigned to the pyridine adduct **7** grow during the decay of *O*-chelate **6** (Figure 5). The assignment of the peaks for the pyridine adduct **7** is consistent with the peak intensity dependence on pyridine concentration (Figures 5 and 6) and the computed CO frequencies relative to those of **4** and **6** (Table 1 and Figure 24S, Supporting Information). Even in the presence of 100 mM pyridine, the observed rate constant for the decay of *O*-chelate **6** (3.8×10^{-3} s^{-1}, a bimolecular substitution) is slower than the observed rate constant for the decay of *O*-chelate **2** (7×10^{-3} s^{-1}, a unimolecular rearrangement).

The results indicate that an *O*-chelate is the first and only intermediate formed after irradiation of **4** and is therefore the precursor to all subsequent species. For example, immediately after steady-state irradiation of **4** in the presence of pyridine, *O*-chelate **6** is observed before pyridine adduct **7** formation, suggesting that pyridine adduct **7** is formed only from **6** and not directly from **4** (Scheme 3). This result is consistent with picosecond to microsecond TRIR studies, where only *O*-chelate **6** is observed (Figure 4). Therefore, as expected, formation of chelate will be much faster than dispersed bimolecular addition. Previous studies show that solvent-coordinated species are converted to a chelate within 200 ns;[1,23] thus, the long-lived

Table 1. CO Stretching Bands of Cymantrene Derivatives in Heptane

	symmetric		asymmetric	
	experimental, cm^{-1} (fwhm)[b]	computational,[a] cm^{-1}	experimental, cm^{-1} (fwhm)[b]	computational,[a] cm^{-1}
1[c]	2024(4)	2035	1943(9)	1975, 1973
2	1947	1982	1887	1943
3	1941	1970	1878	1931
4[d]	2024(4)	2036	1946, 1938(13)	1978, 1970
5[e]	2026(4)	2036	1948, 1940(17)	1978, 1971
6	1948(3)	1980	1887(4)	1941
7	1932	1962	1865(12)	1921
8	1952(3)	1987	1894(5)	1948

[a] Average value for several conformers for **1**, **4**, and **5** (see Discussion for further details). [b] Apparent full width at half-maximum. [c] 3 mM **1** in heptane. [d] 1 mM **4** with 10 mM pyridine in heptane. [e] 0.5 mM **5** in heptane.

Scheme 5. Mechanism of the Decay of **6**

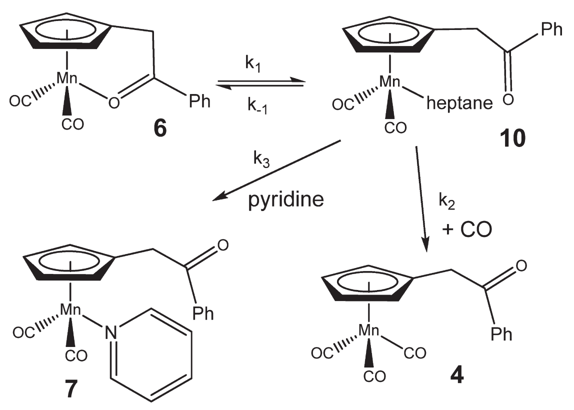

peaks assigned to *O*-chelate **6** are unlikely to be due to a heptane-coordinated intermediate. There is also no evidence of ultrafast solvent coordination similar to that observed for other metal centers that bind to alkane solvents,[1,6b,23−25] suggesting that the chelation excludes ultrafast solvent coordination and that the side chain is in a conformation that favors the ultrafast chelation. It is possible the heptane-coordinated intermediate could be undetected, but only if the heptane-coordinated intermediate and the chelate have identical peaks and the heptane-coordinated intermediate converts only to the chelate.

A mechanism proposed for the decay of **6** is shown in Scheme 5. At low pyridine concentration, the rate of decay of **6** is equal to the rate of formation of **4** (Figure 3). Scheme 5 is consistent with this observation for the steady-state assumptions for recovery of **4** ($k_{-1} \gg k_2[\mathrm{CO}] \gg k_3[\mathrm{pyridine}]$) or formation of **7** ($k_{-1} \gg k_3[\mathrm{pyridine}] \gg k_2[\mathrm{CO}]$; see Supporting Information). At high pyridine concentrations, the rate is first-order in [pyridine], consistent with a steady-state assumption where $k_{-1} \gg k_2[\mathrm{CO}] + k_3[\mathrm{pyridine}]$ and $k_3[\mathrm{pyridine}] \gg k_2[\mathrm{CO}]$. The kinetic results suggest the rate-determining step precedes attack of CO or pyridine and is likely to be the dissociation of the Mn−O bond. If this mechanism is correct, then it also indicates that the formation of *O*-chelate **6** from the solvent-coordinated **10** in Scheme 5 is faster than bimolecular displacement of solvent by a dispersed nucleophile. Nonetheless, a mechanism that excludes **10** where **6** is attacked directly by CO or pyridine is also consistent with the results.

A comparison of **6** with the *O*-chelate **2** is revealing: **2** is thermally unstable ($t_{1/2} \approx 3$ min, 25 °C), as it undergoes a linkage isomerization to the *N*-chelate **3** (Scheme 1).[7] DFT calculations and experimental results suggested that the isomerization occurs via a metal walk along the π system between the two heteroatoms instead of a dissociative mechanism that has a higher barrier (dissociation of the Mn−O bond, followed by rotation of the side chain, and formation of the Mn−N bond).[7] Thus, it appears that the bridge between the two functional groups provides a conduit for rearrangement, and removing the nitrogen in **2** should increase the lifetime of the *O*-chelate since migration along the side chain would not lead to a more stable isomer. Indeed the half-life of *O*-chelate **6** in the absence of added Lewis base ($t_{1/2} = 60$ min, 1948 and 1887 cm^{-1}, Figure 3) is longer than that observed for **2**. Since the *O*-chelate **6** cannot undergo a linkage isomerization to a more stable isomer, the primary path of decay is recombination with carbon monoxide, which results in the recovery of the bleach of **4**. In contrast, allowing the carbon monoxide to escape from solution impedes the decay of *O*-chelate **6**, and the blue chromophore of *O*-chelate **6** is observed even after 24 h (Figure 1). We conclude that the relative stability of an *O*-chelate can increase if a low-energy path to a stable linkage isomer is eliminated.

Formation and Decay of the *O*-Chelate from 5. Steady-state and TRIR results for **5** are similar to those for **4**. Following irradiation of **5** in the absence of added Lewis base, a blue chromophore assigned to the *O*-chelate **8** (A_{704}) has a half-life ($t_{1/2} = 30$ min, Figure 9) that is substantially longer than the half-life for the *O*-chelate **2** ($t_{1/2} = 3$ min at 25 °C),[7] but shorter than the half-life observed for the *O*-chelate **6** ($t_{1/2} = 60$ min, Figure 3). Two factors can contribute to the faster decay of the *O*-chelate **8** versus that of **6**. First, the Mn−O bond in **8** is weakened by the reduced electron density at the side-chain carbonyl (caused by the pyridyl group). Second, even though the *O*-chelate **8** cannot isomerize to an *N*-chelate (a unimolecular process), the pyridyl groups of **5** or *O*-chelate **8** can add to the metal center of another *O*-chelate **8** (both bimolecular processes). Thus, the very broad features at 1920 and 1850 cm^{-1} in Figure 12 are attributed to formation of oligomers where the pyridyl group of one complex adds to the metal center of another and contributes to the decay of *O*-chelate **8**. The lack of an isosbestic point in Figure 9 indicates *O*-chelate **8** does not simply revert back to **5**. This result is supported by FTIR spectra, where the recovery of **5** after irradiation only partially accounts for the decay of peaks assigned to *O*-chelate **8** (1952 and 1894 cm^{-1}, Figure 12). The higher stretching frequencies for *O*-chelate **8** compared to *O*-chelate **6** are attributed to the electron-withdrawing nature of the pyridine ring, which decreases electron donation to the metal and consequently the back-bonding to the metal-CO groups.

On ultrafast time scales, a new absorption peak observed at 1894 cm^{-1} is likewise attributed to the *O*-chelate **8** (Figure 13). The peak has a shoulder near 1885 cm^{-1}, where a peak is often detected for heptane-coordinated complexes.[4,5] This shoulder persists up to 2 μs with no significant decay, but it is gone before standard FTIR spectra can be recorded (several seconds). In previous studies for CpMn and AreneCr complexes, chelation occurs with sulfur- and nitrogen-containing side chains that displace coordinated heptane, and in no case did a heptane-coordinated complex last longer than 200 ns.[1,4,5] We cannot rule out the possibility of a heptane-coordinated complex because the side-chain oxygen may not displace the heptane as effectively as a side chain with sulfur or nitrogen. Nevertheless, no matter how slow the *O*-chelate **8** is formed from a heptane-coordinated complex, the latter is unlikely to persist longer than 100 μs in these experiments because the bimolecular rate constant for solvent displacement is on the order of $10^7\ \mathrm{M}^{-1}\ \mathrm{s}^{-1}$ and the concentration of pyridine groups from **5** and all photoproducts is 1 mM.[4] From these results, one might conclude that a heptane-coordinated complex is not formed from **5**. Likely assignments for the shoulder near 1885 cm^{-1} include transient pyridine σ or π complexes with the pyridine group like those proposed for the irradiation of **1**[7] or pendant pyridine groups on arene chromium carbonyl complexes.[1] We turned to the computational results to explore the plausible structures. None of the computed frequencies for the computed transient unimolecular species match this experimental result. However, the results for the computed red shift of CO frequencies for the heptane-coordinated complex closely match those for the experimentally observed transient: the computed red shift for **8** of 10 to 11 cm^{-1}

in the CO frequency for the model solvent-coordinated complex is very similar to the experimentally observed red shift of 9 cm^{-1} (see Table S3, Supporting Information).

Irradiation of 1. The TRIR spectra for the irradiation of **1** (Figure 14) are distinctly different from those obtained for **4** and **5**. The assignment of two, well-resolved peaks at 1887 and 1878 cm^{-1} to *O*-chelate **2** and *N*-chelate **3**, respectively, is consistent with previous assignments based on steady-state FTIR and NMR experiments and a crystal structure of isolated **3**.[7] As noted above, the assignment of the 1887 cm^{-1} to *O*-chelate **2** is also consistent with the spectra observed for the *O*-chelate **6**.

In the previous study, lower temperatures and shorter irradiation times were used to minimize the rearrangement of **2** to **3**, but a minor amount of **3** was always observed.[7] It was unclear whether both **2** and **3** were directly formed from the excited state of 1, if 3 was formed by secondary photolysis of **2**, or subsequent thermal rearrangement. This distinction is important in determining the mechanism of chelation and the design of selective photochromes. To minimize the possibility of thermal or photoisomerization of **2** to **3** that might occur during steady-state irradiation, TRIR spectroscopy was used with ultrashort laser pulses and time delays. The appearance of *O*-chelate **2** and *N*-chelate **3** in the first 100 ps is limited by vibrational relaxation effects.[22] Assessment of the laser pulse duration, sample absorbance, the pulse intensity, and quantum yields demonstrates that it is impossible for a secondary photolysis to account for rearrangement of **2** to **3** (calculation details are in the Supporting Information). The results suggest that both isomers are formed directly from the excited state of **1** and not by rearrangement of the *O*-chelate **2** to the *N*-chelate **3** because the thermal rearrangement is slow ($\Delta G^{\ddagger} = 20.3$ kcal/mol at 25 °C).[7]

Within experimental error, the relative intensities of **2** and **3** do not change from 10^{-10} to 10 s.[26] Like the product distribution observed for cymantrene derivatives with sulfide side chains,[4,5] the initial distribution of *O*-chelate **2** and *N*-chelate **3** likely depends on thermodynamically favored conformations at the instant a photon is absorbed. The initial chelate distribution is a result of the fact that chelation of proximal functional groups is much faster than solvent coordination and side-chain conformational changes required to form a ring at room temperature.[27]

If solvent coordination were to occur, a transient absorption peak would be expected near 1888 cm^{-1} like that observed for an isooctane-coordinated complex formed following irradiation of methyl cyclopentadienyl manganese tricarbonyl.[28] This peak would overlap the *O*-chelate **6** peak. As noted above, solvent displacement via *N*-chelation should occur within 200 ns,[1] and the latter should result in a change in the relative intensities of the 1887 and 1878 cm^{-1} peaks. Within experimental error, there is no change in these peaks up to several seconds. Therefore, we propose there is no appreciable ultrafast solvent coordination for this system.

Metal Carbonyl Spectra. Metal tricarbonyls normally exhibit two infrared metal−carbonyl stretching peaks where the lower energy peak corresponds to nearly degenerate asymmetric stretching vibrations. For example, both $(\eta^5\text{-}C_5H_5)Mn(CO)_3$[29] (in cyclohexane) and $(\eta^5\text{-}CH_3C_5H_4)Mn(CO)_3$[30] (in *n*-hexane) have CO vibrational stretches at 1944 cm^{-1}, which are substantially broader and larger than their respective stretches at 2027 and 2025 cm^{-1}.[31] In contrast, three CO stretching peaks are observed for **4** and **5** before irradiation (see Figures 19S−22S in the Supporting Information) and after irradiation as bleaches (Figures 3, 5, 6, and 12). We propose that for the lowest energy conformers the interactions of the side chains of **4** and **5** with the metal carbonyl groups are responsible for the loss of near degeneracy of the two asymmetric stretching frequencies. A much larger interaction for **4** and **5** compared to **1** is supported by the larger frequency differences determined computationally (Table 1).[32] This interpretation is consistent with the observation that these complexes undergo ultrafast chelation, which requires that the side-chain functional group must be near the metal center at the instant of CO dissociation.

■ SUMMARY

Three cyclopentadienyl manganese tricarbonyl derivatives, **1**, **4**, and **5**, with different side chains ($Mn\{\eta^5\text{-}C_5H_4CH_2COR\}(CO)_3$, R = 2-pyridinyl **1**, phenyl **4**, and 4-pyridinyl **5**) have been prepared and studied. The species formed following UV irradiation of **1**, **4**, and **5** have been characterized and identified with both experimental (FTIR, TRIR, UV−vis, and NMR) and computational (DFT) techniques. Photodissociation of CO from model compounds **4** and **5** produces *O*-chelates **6** and **8**, respectively, within 100 ps. In the case of **5**, there is evidence of ultrafast formation of another species, and the infrared peaks are consistent with a solvent-coordinated species, but kinetic data indicate this assignment is unlikely. The *O*-chelates **2**, **6**, and **8** each decay on minute time scales in the presence of added or pendant pyridine groups, but in the absence of any pyridine group the *O*-chelate **6** persists for 24 h. Photodissociation of CO from **1** produces simultaneously *O*-chelate **2** and *N*-chelate **3** within 100 ps. Because the observation of metal carbonyl species is limited by vibrational relaxation (ca. 100 ps), this time scale is the upper limit for the formation of the chelates **2** and **3**. Importantly, ultrafast solvent coordination can occur within a few picoseconds and provides a benchmark for the rate of ultrafast chelation: if ultrafast solvent coordination is limited by competing ultrafast chelation, then the chelation is almost certainly occurring in less than a picosecond. These are the time scales that will ensure optimum performance of optically driven molecular devices.

■ ASSOCIATED CONTENT

S Supporting Information. Time-resolved UV spectra, plots of $\ln(A_0/A_t)$ from UV spectra, IR spectra of **1**, **4**, and **5**, kinetic derivations for Scheme 5, details for computational results for CO frequencies, and computed energies of stationary points related to **8**. This material is available free of charge via the Internet at http://pubs.acs.org.

■ AUTHOR INFORMATION

Corresponding Author

*E-mail: cewebstr@memphis.edu; tburkey@memphis.edu.

■ ACKNOWLEDGMENT

This work was partly supported by the National Science Foundation under Grant No. CHE-0911528 (T.J.B. and C.E.W.) and the National Institute of Standards and Technology under Award No. 70NANB8H129 (T.J.B.).

■ REFERENCES

(1) To, T. T.; Heilweil, E. J; Duke, C. B., III; Ruddick, K. R.; Webster, C. E.; Burkey, T. J. *J. Phys. Chem. A* **2009**, *113*, 2666–2676.

(2) The upper limit was determined by the resolution of the instrument response: Sorensen, A. A.; Yang, G. K. *J. Am. Chem. Soc.* **1991**, *113*, 7061–7063.

(3) Pang, Z.; Burkey, T. J.; Johnston, R. F. *Organometallics* **1997**, *16*, 120–123.

(4) Jiao, T.-J.; Pang, Z.; Burkey, T. J.; Johnston, R. F.; Heimer, T. A.; Kleinman, V. D.; Heilweil, E. J. *J. Am. Chem. Soc.* **1999**, *121*, 4618–4624.

(5) (a) To, T. T; Burkey, T. J.; Heilweil, E. J. *J. Phys. Chem. A* **2006**, *110*, 10669–10673. (b) To, T. T; Duke, B. C., III; Burkey, T. J.; Heilweil, E. J. *J. Phys. Chem. A* **2007**, *111*, 6933–6937. (c) Yeston, J. S.; To, T. T; Burkey, T. J.; Heilweil, E. J. *J. Phys. Chem. B* **2004**, *108*, 4582–4585.

(6) (a) Xie, X.; Simon, J. D. *J. Am. Chem. Soc.* **1990**, *112*, 1130–1136. (b) Joly, A. G.; Nelson, K. A. *Chem. Phys.* **1991**, *152*, 69–82. (c) Joly, A. G.; Nelson, K. A. *J. Phys. Chem.* **1989**, *93*, 2876–2878. (d) Simon, J. D.; Xie, X. *J. Phys. Chem.* **1987**, *91*, 5538–5540. (e) Simon, J. D.; Xie, X. *J. Phys. Chem.* **1986**, *90*, 6751–6753. (f) Kotz, K. T.; Yang, H.; Snee, P. T.; Payne, C. K.; Harris, C. B. *J. Organomet. Chem.* **2000**, *596*, 183–192.

(7) To, T. T.; Duke, C. B.; Junker, C. S.; O'Brien, C. M.; Ross, C. R.; Barnes, C. E.; Webster, C. E.; Burkey, T. J. *Organometallics* **2008**, *27*, 289–296.

(8) Rybinskaya, M. I.; Korneva, L. M. *J. Organomet. Chem.* **1982**, *231*, 25–35.

(9) Telegina, L. N.; Ezernitskaya, M. G.; Godovikov, I. A.; Babievskii, K. K.; Lokshin, B. V.; Strelkova, T. V.; Borisov, Y.; Loim, N. M. *Eur. J. Inorg. Chem.* **2009**, 3636–3643.

(10) Brown, G. H. *Photochromism*; Wiley: New York, 1971.

(11) Certain commercial equipment, instruments, or materials are identified in this paper to adequately specify the experimental procedure. In no case does identification imply recommendation or endorsement by NIST, nor does it imply that the materials or equipment identified are necessarily the best available for the purpose.

(12) Frisch, M. J.; Trucks, G. W.; Schlegel, H. B.; Scuseria, G. E.; Robb, M. A.; Cheeseman, J. R.; Scalmani, G.; Barone, V.; Mennucci, B.; Petersson, G. A.; Nakatsuji, H.; Caricato, M.; Li, X.; Hratchian, H. P.; Izmaylov, A. F.; Bloino, J.; Zheng, G.; Sonnenberg, J. L.; Hada, M.; Ehara, M.; Toyota, K.; Fukuda, R.; Hasegawa, J.; Ishida, M.; Nakajima, T.; Honda, Y.; Kitao, O.; Nakai, H.; Vreven, T.; Montgomery, Jr., J. A.; Peralta, J. E.; Ogliaro, F.; Bearpark, M.; Heyd, J. J.; Brothers, E.; Kudin, K. N.; Staroverov, V. N.; Kobayashi, R.; Normand, J.; Raghavachari, K.; Rendell, A.; Burant, J. C.; Iyengar, S. S.; Tomasi, J.; Cossi, M.; Rega, N.; Millam, N. J.; Klene, M.; Knox, J. E.; Cross, J. B.; Bakken, V.; Adamo, C.; Jaramillo, J.; Gomperts, R.; Stratmann, R. E.; Yazyev, O.; Austin, A. J.; Cammi, R.; Pomelli, C.; Ochterski, J. W.; Martin, R. L.; Morokuma, K.; Zakrzewski, V. G.; Voth, G. A.; Salvador, P.; Dannenberg, J. J.; Dapprich, S.; Daniels, A. D.; Farkas, Ö.; Foresman, J. B.; Ortiz, J. V.; Cioslowski, J.; Fox, D. J. *Gaussian 09*, Revision A.02; Gaussian, Inc.: Wallingford, CT, 2009.

(13) (a) Perdew, J. P.; Burke, K.; Ernzerhof, M. *Phys. Rev. Lett.* **1996**, *77*, 3865–3868. (b) *Erratum* **1997**, *78*, 1396.

(14) Parr, R. G.; Yang, W. *Density Functional Theory of Atoms and Molecules*; Oxford University Press: New York, 1989.

(15) (a) Hay, P. J.; Wadt, W. R. *J. Chem. Phys.* **1985**, *82*, 299–310. (b) Wadt, W. R.; Hay, P. J. *J. Chem. Phys.* **1985**, *82*, 284–298.

(16) Couty, M.; Hall, M. B. *J. Comput. Chem.* **1996**, *17*, 1359–1370.

(17) Ehlers, A. W.; Böhme, M.; Dapprich, S.; Gobbi, A.; Höllwarth, A.; Jonas, V.; Köhler, K. F.; Stegmann, R.; Veldkamp, A.; Frenking, G. *Chem. Phys. Lett.* **1993**, *208*, 111–114.

(18) Hariharan, P. C.; Pople, J. A. *Theor. Chim Acta* **1973**, *28*, 213–222. The 6-31G(d′) basis set has the d polarization functions for C, N, and O taken from the 6-311G basis set, instead of the original arbitrarily assigned value of 0.8 used in the 6-31G(d) basis set. Foresman, J. B.; Frisch, Æ. *Exploring Chemistry with Electronic Structure Methods*, 2nd ed.; Gaussian, Inc.: Pittsburgh, PA, p 110.

(19) Francl, M. M.; Pietro, W. J.; Hehre, W. J.; Binkley, J. S.; DeFrees, D. J.; Pople, J. A.; Gordon, M. S. *J. Chem. Phys.* **1982**, *77*, 3654–65.

(20) (a) Dunlap, B. I.; Connolly, J. W. D.; Sabin, J. R. *J. Chem. Phys.* **1979**, *71*, 3396–3402. (b) Dunlap, B. I.; Connolly, J. W. D.; Sabin, J. R. *J. Chem. Phys.* **1979**, *71*, 4993–4999. (c) Dunlap, B. I. *J. Chem. Phys.* **1983**, *78*, 3140–3142. (d) Dunlap, B. I. *J. Mol. Struct. (THEOCHEM)* **2000**, *529*, 37–40.

(21) We speculate that the nonexponential decay observed in the absence of pyridine is an autocatalytic reaction resulting from multinuclear products whose formation are otherwise inhibited by excess pyridine.

(22) See ref 7 and Supporting Information.

(23) (a) To, T. T.; Heilweil, E. J.; Duke, C. B., III; Burkey, T. J. *J. Phys. Chem. A* **2007**, *111*, 6933–6937. (b) Yeston, J. S.; To, T. T.; Burkey, T. J.; Heilweil, E. J. *J. Phys. Chem. B* **2004**, *108*, 4582–4585.

(24) Dougherty, T. P.; Heilweil, E. J. *Chem. Phys. Lett.* **1994**, *227*, 19–25.

(25) Schwartz, B. J.; King, J. C.; Zhang, J. Z.; Harris, C. B. *Chem. Phys. Lett.* **1993**, *203*, 503–508.

(26) Since **2** can be observed by FTIR at room temperature, there can be no process that would cause the decay of **2** in one second or less. In general the variations observed in peak intensities in Figure 14 on ultrafast time scales are due to random or experimental error. This fact is apparent when additional spectra are examined (Figures 26S and 27S in the Supporting Information). The bleach near 1940 cm^{-1} is variable partly due to the fact that the laser intensity varies, especially for ns vs ps spectra, since different lasers were used to obtain optimum signal-to-noise. The variation in bleach intensity leads to variation in the apparent position of overlapping peaks.

(27) Winnik, M. A. *Chem. Rev.* **1981**, *81*, 491–524.

(28) DeWitt, K.; To T. T.; Heilweil, E. J. *Unpublished result*. The only published results are for related cymantrene derivatives where *n*-hexane-coordinated species from acyl derivatives of cymantrene are observed at 1906−1910 cm^{-1}. See refs 4 and 5c.

(29) Lugovskoy, S.; Lin, J.; Schultz, R. H. *J. Chem. Soc., Dalton Trans.* **2003**, 3103–3110.

(30) Weber, L.; Domke, I.; Stammler, H.-G.; Neumann, B. *Eur. J. Inorg. Chem.* **2005**, 4715–4722.

(31) Similar data have been reported: (a) Parker, D. J.; Stiddard, M. H. B. *J. Chem. Soc. A* **1968**, 2263–2264. (b) Haines, L. M.; Stiddard, M. H. B. *Adv. Inorg. Chem. Radiochem.* **1969**, *12*, 53–133.

(32) The tabulated computed frequencies for **1**, **4**, and **5** are averaged values from three, three, and two optimized conformers, respectively, with very similar relative energies and frequencies within each set. See Supporting Information for further details.